35. L. J. Cohen and H. M. Berkowitz, "Time dependent fracture criteria for 6061-T6 aluminum under stress-wave loading in uniaxial strain," Int. J. Fracture Mech., 7, No. 2 (1971).
36. S. A. Novikov, I. I. Divnov, and A. G. Ivanov, "Investigation of the rupture of steel, copper, and aluminum under explosive loading," Fiz. Met. Metalloved., 21, No. 4 (1966).
37. S. A. Novikov, Yu. S. Sobolev, et al., "Investigation of the influence of the temperature on the magnitude of the rupture stress during spall in copper," Probl. Prochn., No. 3 (1977).
38. N. A. Zlatin, G. S. Pugachev, et al., "Time dependence of the strength of metals for microsecond band longevities," Fiz. Tverd. Tela, 17, No. 9 (1975).
39. Yu. V. Bat'kov, S. A. Novikov, et al., "Influence of the specimen temperature on the magnitude of the rupture stress during spall in the aluminum alloy AMg-6," Zh. Prikl. Mekh. Tekh. Fiz., No. 3 (1979).

MODELING OF SPALLING RUPTURE UNDER SHOCK DEFORMATION. ANALYSIS OF AN INSTANTANEOUS SPALLING SCHEME

N. Kh. Akhmadeev and R. I. Nigmatulin

UDC 539.42:620.172.254

1. Spalling of the rear part of a specimen being loaded [1, 2] is observed during shock or explosive loading of metal targets when the shock being generated is of sufficient intensity and emerges on the free surface. Experimental investigations of this phenomenon in [3, 4] are devoted mainly to the determination of the time dependence of the specimen strength in the spall section for loads of duration $\sim 10^{-6}$ sec. On the basis of the data from these experiments, one of the deductions [4] is the determination of the spalling rupture process as a multifocus process, when there occur a large number of microcracks in the tensile force zone, which merge in their further development into a single large crack separating the specimen into two parts. A group of papers [1, 5-8] represents the results of experimental investigations of spalling rupture stresses under shock and explosive deformation of specimens of different materials. Analysis of these papers results in the following fundamental conclusion: For each of the materials tested there is a significant spread in the calculated (by acoustic theory) values of the spalling rupturing stresses, that vary substantially as a function of the experiment conditions. Part of the spall experiments (see [6, 9], say) is devoted to determining the threshold values of the impactor flight velocity corresponding to the origination of initial damage (or micropores, microcracks) in the tension wave, and to the formation of total spalling rupture. It should be noted that because of the great complexity and for a more unique treatment, the experiments are performed mainly in a plane formulation permitting the clarification of the most characteristic features of the phenomenon being studied. Considerable difficulties must also be encountered in a numerical modeling of the shock and explosive loading of specimens. The mathematical models proposed for the nonstationary shockwave flows are a system of nonlinear partial differential equations, and they can be investigated completely only by using powerful computers.

Especially necessary in a numerical investigation of the propagation of an initiated shock pulse is taking correct account of the different physicochemical processes occurring in the shocks and the rarefaction waves — for instance, taking account of the elastic-plastic and phase transitions resulting in the formation of a multiwave profile of the shock pulse, taking account of wave interaction on the contact and free boundaries, etc. The shock loading method and the history of flow development can alter the whole wave pattern to a significant extent. Hence, constant correlation of the results of a computation with the data of full-scale tests is necessary. An elastic-plastic model of a two-phase continuous medium with physicochemical transformations is developed in [10, 11], that permits modeling processes occurring during the high-speed collision of two plates of length l_1 and l and complicated by phase transformations. Modeling the motion of detonation waves and the loading process of iron and nickel specimens by the explosion of a superposed high-explosive charge of crystalline and porous hexogen is executed in [12, 13]. On the basis of the elastic-plastic model proposed in [10, 11], a numerical investigation is performed in this paper for the process

Ufa and Moscow. Translated from Zhurnal Prikladnoi Mekhaniki i Tekhnicheskoi Fiziki, No. 3, pp. 120-128, May-June, 1981. Original article submitted March 19, 1980.

0021-8944/81/2203-0394$07.50

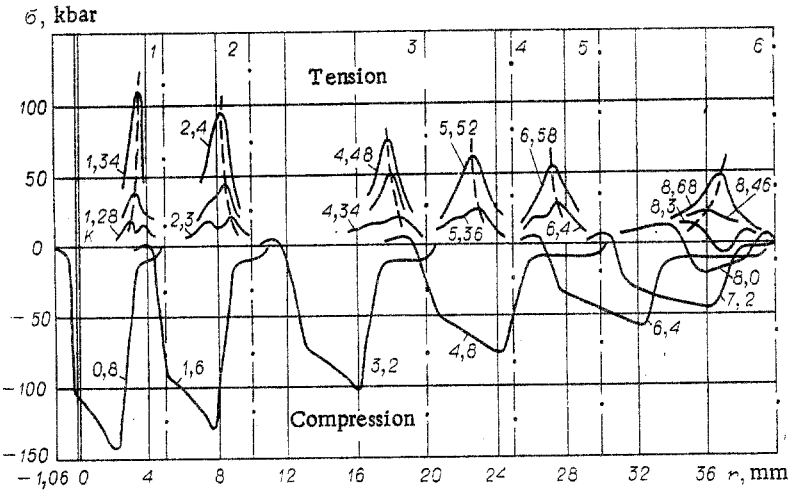

Fig. 1

of shock loading a steel target by using an impactor, and for the origination of an instantaneous spalling rupture during interaction of the opposite unloading waves.

2. The fundamental equations of an elastic-plastic two-phase model in a one-velocity and one-temperature approximation for the plane case are a system of differential equations of mass conservation of the first and second phases and the equations of momentum and energy conservation for the whole mixture [11]. We represent the equations of the model in Lagrange coordinates in the form

$$\begin{gathered}(\rho_0/\rho)\partial\rho_1/\partial t + \rho_1\partial u/\partial r + (\rho_0/\rho)J_{12} = 0,\\ (\rho_0/\rho)\partial\rho_2/\partial t + \rho_2\partial u/\partial r - (\rho_0/\rho)J_{12} = 0,\\ \rho_0\partial u/\partial t = \partial\sigma^{11}/\partial r, \quad \rho_0/\rho\,[\rho_1\partial e_1/\partial t + \rho_2\partial e_2/\partial t + (e_2 - e_1)J_{12}] = \sigma^{11}\partial u/\partial r,\end{gathered} \tag{2.1}$$

where ρ, ρ_i, ρ_i^0 are the mean density of the mixture, and the mean and true density of the i-th phase, J_{12} is the velocity of the phase transitions, e_i is the specific internal energy of the i-th phase, and u is the mass flow rate. We represent the stress tensor σ^{11} to describe flows in elastic-plastic media as the sum of gyrostatic and deviator parts

$$\sigma^{11} = -p(\rho_i^0, T) + \tau^{11}, \tag{2.2}$$

where p is the gyrostatic pressure dependent on the true density ρ^0 and the temperature T, and τ^{11} is the stress deviator for which Hooke's law is valid:

$$d\tau^{11}/dt = {}^4/_3\mu(\rho/\rho_0)\partial u/\partial r. \tag{2.3}$$

Plastic flow starts when the deviator τ^{11} reaches the yield point τ^* (under simple tension or compression), and furthermore, in conformity with the Mises flow condition the condition of conservation of the deviator at the yield point, i.e., $\tau^{11} = \tau^*$, should be satisfied. The change in the strength properties of a medium as a function of the shock intensity is taken into account by the linear relationship

$$\tau^* = \tau_0^* + M(p - p_0),$$

where τ_0^*, p_0 is the yield point and the pressure at the Hugoniot point on the shock adiabat at which the transition occurs from the elastic to the plastic flow mode; a linear dependence on the density ρ^0 is usually used for the shear modulus μ [10].

The appearance of cracks or spalls of the material being subjected to unloading by tensile stresses can be taken into account in the model being proposed. The formation of an instantaneous mainline spall crack upon the achievement of a certain critical spall stress σ_* is considered as a first approximation for the origination of tensile stresses in the interaction domain of opposite unloading waves. It is considered that at this point l_* (unknown beforehand), where the condition $\sigma^{11} > \sigma_*$ is satisfied, rupture of the continuity of substance occurs simultaneously along the whole section, as does separation of the specimen into two parts with the formation of a free surface on which $\sigma^{11}(l_*, t) = 0$. Such a schematization is perfectly valid for the interaction between opposite unloading shocks (on which

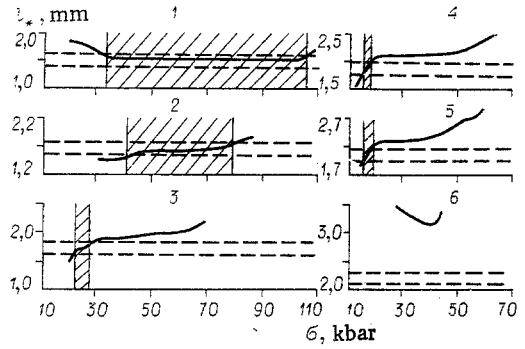

Fig. 2

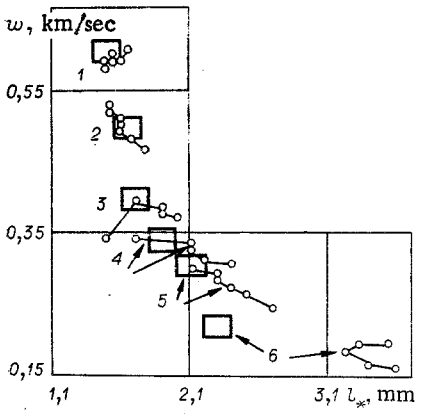

Fig. 3

the reverse phase transformations are realized), when so-called principal spalls occur in extremely narrow zones [14].

The recoil of the impactor from the target as soon as tensile stresses appear on the contact surface, i.e., for $\sigma^{11}(l_1, t) > 0$, should also be provided for in loading schemes with the collision of plates. From this time, l_1 is a free surface, and $\sigma^{11}(l_1, t) = 0$. As specially formulated numerical experiments showed, not taking account of the impactor recoil can substantially distort the unloading wave at the target, moving away from the impactor, in quantitative respects, and this will, in turn, strongly influence the formation of the rupturing pulse of tensile stresses.

The system (2.1)-(2.3) is closed by the equation of state of the mixture phases, which was used in the Mie–Gruneisen form [11], and by the condition of combined phase deformation when

$$p_1(\rho_1^0, T) = p_2(\rho_2^0, T).$$

Let us note that for substances in which there are no phase transformations in shocks, the second equation in (2.1) drops out, and the relations (2.1)-(2.3) describe the behavior of a single-phase substance. The phase transformation kinetics was given by the results from [11] in an examination of shocks in iron or low-carbon steel specimens, and a method of numerical (through) computation of shock propagation is elucidated briefly there with the introduction of artificial viscosity in the shock compression zones.

3. The model considered above with the scheme presented for instantaneous spall was used to model the conditions of a series of experiments [15] in which a steel plate (l_1 = 1.06 mm, V_0 = 0.96 km/sec) collided with St. 3 targets of different length, namely, 5, 10, 20, 25, 30, and 40 mm, for the numerical investigation of spalling rupture. The diameter of the colliding plates was 120 mm in the first three tests, and 150 mm in the last three. This series of tests in [15] is selected to include a large range of target lengths (from very short to very long), realized for fixed shock velocities and impactor lengths. The following parameters of a spall plate were measured in the tests: the length l_* and mean flight velocity w. The critical rupturing stress, equal to ~80 kbar, was calculated in an acoustic approximation from the results of the measurements. Results of a numerical modeling of the shock loading of targets are represented in Fig. 1 as a diagram of the stress $\sigma(r)$ at different times t for all six tests, under the assumption that the strength of the specimens being tested is sufficiently high so as to clarify the nature of tensile stress formation for all allowable stresses being realized under the conditions for the selected series of experiments [15]. The dash-dot lines, marked by the ordinal number of the test, show the location of the free target surfaces in tests 1-6 around which the appropriate tensile stress pulses are formed (upon reflection of the incident shock). The dash-dot lines mentioned cut off a distance equal to the appropriate target length on the r axis. It is seen from the computational data presented that the compression shock being formed (after collision of the plates) attenuates to a significant extent as it advances into the target bulk, the shock amplitude is practically halved (see the diagram for t = 0.8 and 6.4 μsec), and the width of the wave approximately doubled, on the other hand. Computations showed that $\alpha \rightleftarrows \varepsilon$ phase transformations in the target occur in a shock only in the first 4-6 mm from the contact surface, and although they do not occur in the total volume, nevertheless in a control version

of the computation (without phase transitions) it is clarified that it is impossible to neglect the influence of phase transformation on shock evolution. The process of shock reflection from a free surface is shown in Fig. 1 for the longest target (test 6, l = 40 mm). The tensile and attenuated shock (see the diagram of $\sigma(r)$ for t = 7.2 μsec in Fig. 1) forms a strongly spread out tension pulse upon reflection from the free surface, whose growth rate is relatively small. Formation of a tensile pulse occurs here between t = 8.30 and t = 8.68 μsec, then attenuation of the effect of the tensile stresses and tension wave motion from the free surface occur. It follows from the results in Fig. 1 that the maximal tensile stresses σ = 114, 96, 74, 64, 56, and 46 kbar, are respectively possible in experiments 1-6, and are achieved in the times τ = 0.06, 0.10, 0.14, 0.16, 0.18, and 0.22 μsec after the appearance of the tensile stresses $\sigma \approx 20$ kbar.

The numerical results represented demonstrate sufficiently graphically the process of tensile pulse formation as a function of the change in target length for other conditions remaining fixed. The parameters of the shock pulse incident on the free surface, the maximum value of the pulse amplitude and width, and the configuration of the pulse leading and trailing profiles are governing in the formulation of spalling rupture. In all six experiments, two local maxima which gradually come together and later grow into one maximum are formed on the curves $\sigma(r)$ in Fig. 1 in the unloading zone. The greatest tensile stresses $\sigma_*(r, t)$ achieved at each instant are marked by dashed lines. The left maximum is greater than the right in the first and sixth experiments. This is caused in the first case by the arrival of a short and strong shock pulse in the first case, and in the sixth by the fact that a strongly spread out and considerably attenuated shock pulse arrived at the free surface. It follows from Fig. 1 (see the dashed lines) that if a certain quantity σ_* is given (for which spall occurs as soon as it is reached), then as σ_* increases to a definite limit the quantity l_* will diminish in tests 1 and 6 and on the other hand increase in tests 2-5. By knowing the experimental value of l_* and constructing the computed dependence of σ_* on l_*, it is possible to try to clarify whether there is a certain single value of the spalling rupturing stress σ_* which would simultaneously satisfy all the experiments, or by finding the domain of allowable values of spall stresses σ_* in each experiment, would it be possible to isolate a common zone of critical stresses σ_* from them. The authors of this paper were guided by precisely these considerations in the initial formulation of the numerical experiments.

Results of comparing experimental and computed spall lengths l_* as a function of the tensile stresses σ are represented in Fig. 2 for all six tests. The dashed lines show the allowable values of the experimentally measured spall plate lengths with the limits for the errors in measuring l_* indicated in [15] taken into account. The continuous line is the numerical results, the hatched domain is the domain of possible spalling stresses σ_*. The results of the comparison indicate that if the spall plate length l_* is determined with sufficient accuracy in experiments, then there is no single zone of intersection between all the domains found for possible σ_* and there is no single critical stress σ_* which could be used to make all the experiments of the series under consideration agree. Moreover, a large number of the test computations performed also showed that upon being given a certain single value of σ_*, it is impossible to make computation and experiment agree satisfactorily. An analysis of the papers [1, 5-8] in which critical rupturing stresses were calculated from measurement data confirms this same deduction. Taking account of existing experimental facts, the present results afford a possibility of formulating the following deduction: its own value of σ_*, dependent on the specific conditions of the experiment, is realized in each experiment. For tests in which a comparatively rapid growth of the tensile pulse is observed, in the time $\tau \leqslant 0.10$ μsec after appearance of tensile stresses $\sigma \approx 20$ kbar (see tests 1 and 2 in Figs. 1 and 2), the critical spall stress is realized for $\sigma > 40$ kbar. Computations showed that the spall stress σ_* = 60 kbar describes tests 1 and 2 well. As the time of tensile stress growth increases, the quantity σ_* decreases and for $\tau \approx 0.20$ μsec (see tests 4, 5, and 6 in Figs. 1 and 2) σ_* is of the order of 20 kbar.

Attention should be turned to the sixth experiment in which the experimental length l_* is possibly substantially reduced. This same tendency is followed, although to a lesser degree, for tests 4 and 5, which differ from the first three by a rather exaggerated diameter of the colliding plates. Let us note that in the experiments with explosive loading [15] of St. 3 obstacles, as the length of the obstacle l varied in the same range from 5 to 40 mm, the quantity l_* increased correspondingly from 1.5 to 5 mm. As is shown in [13], loading schemes with a superposed high-explosive charge result in the formation of a stretched-out triangle

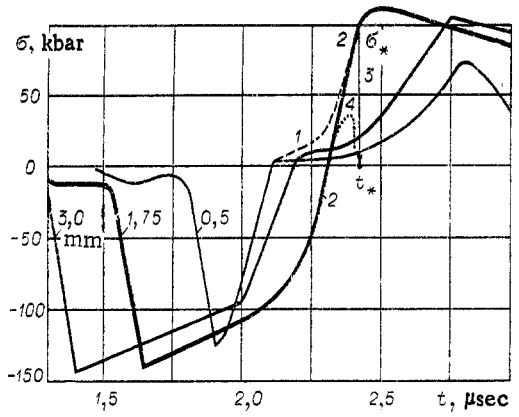

Fig. 4

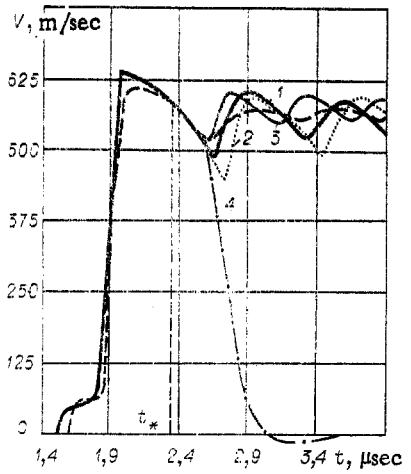

Fig. 5

of the shock pulse in the obstacle with a spread-out unloading wave profile and more rapid shock attenuation than during the collision of plates. In experiments [15] with the impact of a plate, the length of the spall plate l_* varies from 1.5 to 2.2 mm for the same target lengths, and there are generally no special reasons for such an abrupt diminution in l_* (from 5 to 2.2 mm) in long targets as a function of the change in the loading method. Results of comparing the computed and experimental data on two parameters controllable in the experiment, the length l_* and the mean velocity of the plate flight w, are shown in Fig. 3. Experimental results [15] with the stipulated errors in measuring l_* and w taken into account are superposed in the form of rectangles, and results of a numerical modeling of the spall of a plate obtained each time for different σ_* by circles. As before, the computation and experiment for the first three tests correlate sufficiently well, rather worse for the fourth and fifth tests, and there is a significant discrepancy for the sixth test. The results in Fig. 3 show that more real values of l_* for tests 4, 5 and 6 are values for their lower bound of 2.1, 2.4, and 3.3 mm, respectively, for which $\sigma_* \approx 35$ kbar. Discussion of this discrepancy between the computation and the test with the author of the experiment [15] showed that in long targets (~30-40 mm) the spall is characterized by the formation of a porous structure in layers lying closest to the spall surface, where the width of the porosity zone increases with the increase in the target length (for a fixed material, impactor length, and shock velocity); short targets are characterized by a rough spalling surface. The length of the plate in [15] was calculated by the mass of the conserved part being spalled with an appropriate reduction to the mass of a continuous specimen. Losses of some mass of the plate during spall formation and not taking account of the presence of a porous zone around the spall plane (up to 20% of l_*) could result in the reduction of the length l_* of the spall plate in [15].

4. The instantaneous spall model considered above was also used in application to the conditions of an experiment [7] in which an aluminum plate (l_1 = 2 mm, V_0 = 1.31 km/sec) and a low-carbon steel plate (l = 9.9 mm) collided with a plane collision diameter of 50 mm. Oscillograms of the velocity of the rear free target surface were obtained with good accuracy by a capacitive transducer in [7], and what is quite important, several fluctuations in the free surface velocity were determined for the spall plate which had already separated from the target. This permitted making a detailed qualitative and quantitative analysis of the experimental velocity profile of the target free surface V(t) in [7]. The value of this experiment for the purposes of this paper is, as before, that it permits comparing the results of numerical experiments on the change in the target free surface velocity, and then on the part being spalled directly with the data of the test oscillogram. Model experiments were performed for targets of length l = 9.9 mm, in which all the processes that occur can be considered planar with a great degree of reliability. The computed data showed that the nature of the shock flow development for the conditions of the experiment in [7] is close to the data of the test 2 of the experiment examined earlier [15] (see the σ(r) diagram for test 2 in Fig. 1). The process of tensile stress pulse formation is also characterized by the formation of two local maxima that then grow into one maximum at a depth of ~1.75 mm from the outer free surface of the target.

Computed dependences of the stress σ on the time t are represented in Fig. 4 for several fixed target sections marked by numbers corresponding to the distance of a section from the external (free) surface of the target in millimeters. It is seen that the greatest growth in the tensile stresses (and the greatest strain rate correspondingly) is at the depth 1.75 mm (curve 2), and in precisely this section it is completely possible to expect the formation of a mainline crack and the spalling of part of the target of length $l_* = 1.75$ mm, which is in agreement with the results of the experiment [7]. The data represented in Fig. 4 indicate the strong dependence of the magnitude of the critical rupturing stresses in the spall section on the time of their action and on the strain rate. Here the more rapid the unloading, the higher the rupturing stresses that can be reached by the material because of overstretching which is possible because of a certain lag in crack formation.

An instantaneous spall diagram is displayed by lines 1-3 in Fig. 4. From the time of the appearance of tensile stresses, a point corresponding to the maximum of the tensile $\sigma_*(r, t)$, reached at each time t by different target depths, moves along the dashed line 1 which then goes over into the curve 2. On reaching a given separation stress σ_* at the time t_*, instantaneous spall occurs (along the line 3), and the formation of a free surface and, besides, the stress $\sigma(l_*, t) = 0$ for $t > t_*$. If it is taken into account that the spall zone is characterized by damage formation, microcracks, and micropores, which are sources for the reduction of the effective stresses [16], then growth of the tensile stresses in time will be less in the spall section (for instance along line 4), than along the solid substance (line 2). Its position changes towards diminishing σ and the growth curve of the maximal tensile stresses $\sigma_*(t)$ towards line 1. The specific form of the dependence $\sigma(r, t)$ in the rupture zone is determined by the kinetics of microdamage formation and growth.

As is seen from Fig. 4, as the value of the separating stress σ_* varies, different values of the spall depth can be obtained. However, it is not clear beforehand whether the complex of computed quantities σ_*, l_* and fundamental characteristics of the time dependence V(t) of the flying spall plate will satisfy the data of full-scale experiments. In this connection, a number of computations have been performed for the conditions of the experiment in [7], in which the velocity of the outer free surface of the target was specially tracked. The numerical free surface velocity profiles obtained for the target in the computations and its part being spalled are represented in Fig. 5 in the form of the lines 1, 3, and 2, and the comparable experimental profile V(t) from [7] is shown by dashes. The computed profile of the free surface velocity profile for a target not experiencing spall under tension is marked by the dash-dot line 4. The computed spall time after collision $t_* = 2.36$ μsec is shown by the vertical dashed line on the t axis and on the profile V(t). The best approximation to the experiment in [7] is obtained when $\sigma_* = 50$ kbar (curve 1). Comparison of the period of vibrations V(t) and the mean value of the plate flight velocity w with the test curve indicates the values of l_* and w that agree completely with test. Approximate computations showed (curves 2 and 3 in Fig. 5) that an increase in σ_* results in still greater mismatch between the values of the oscillation amplitude V(t) after spall (line 2 corresponds to $\sigma_* = 70$ kbar), but here the mean velocity of the flying plate w diminishes because a certain part of the pulse would still succeed in going over to the target for a rise in σ_*. At the same time l_* and the period of the fluctuation would increase, and the diminution of σ_* (line 3 in Fig. 5 corresponds to $\sigma_* = 40$ kbar) will result in an increase in w and a diminution in the amplitude of the oscillation V(t) of the length of the spall plate l_*, and of the period of fluctuation. The available relatively small difference between the computed (curve 1 for $\sigma_* = 50$ kbar) and experimental amplitudes of the velocity fluctuations V(t) is completely explainable if it is taken into account that the spall process can occur along line 4 of Fig. 4 (because of the influence of microdamage).

Therefore, the results represented above show that the instantaneous spall scheme examined will satisfactorily describe the spall being realized during a rapid growth of the tensile stresses in sufficiently strong waves with stresses on the order of 80 kbar (for instance, during collisions of intense unloading waves, experiments 1 and 2 in [15] and the experiment examined in [7]). To describe spalls in waves of lesser intensity (for example, experiments 3-6 in [15]), characterized by the formation of microdefects during the action of a tensile stress pulse, it is necessary to introduce the kinetics of formation and accumulation of microcracks and micropores, which are sources of reduction of the acting stresses.

The authors are grateful to G. I. Kanel' and A. M. Molodets for useful discussion, as well as to M. G. Stadnik and A. T. Khamatdinova for assistance in performing the numerical experiments.

LITERATURE CITED

1. S. A. Novikov, I. I. Divnov, and A. G. Ivanov, "Investigation of the rupture of steel, aluminum, and copper under explosive loading," Fiz. Met. Metalloved., 21, No. 4 (1966).
2. I. C. Skidmore, "Introduction to shock waves in solids," Appl. Mater. Res., 4, No. 3 (1965).
3. N. A. Zlatin, S. M. Mochalov, et al., "Time regularities of the metal rupture process under intensive loads," Fiz. Tverd. Tela, 16, No. 6 (1974).
4. N. A. Zlatin, G. S. Pugachev, et al., "Time dependence of metal strength for microsecond range longevities," Fiz. Tverd. Tela, 19, No. 9 (1975).
5. L. V. Al'tshuler, S. A. Novikov, and I. I. Divnov, "Relation between the critical rupturing stresses and the time of rupture in explosive deformation of metals," Dokl. Akad. Nauk SSSR, 166, No. 1 (1966).
6. B. M. Butcher, L. M. Barker, et al., "Influence of stress history on time-dependent spall in metals," AIAA J., 2, No. 6 (1964).
7. A. M. Molodets, "Measurement of the spall strength of three steels," in: Detonation. Critical Phenomena. Physicochemical Transformations in Shocks [in Russian], Chernogolovka (1978).
8. B. A. Tarasov, "Resistance of plates to rupture under shock loading," Probl. Prochn., No. 3 (1974).
9. B. A. Tarasov, "On a quantitative description of spall damage," Zh. Prikl. Mekh. Tekh. Fiz., No. 6 (1973).
10. R. I. Nigmatulin, "Model of motion and shocks in two-phase solids with phase transitions," Zh. Prikl. Mekh. Tekh. Fiz., No. 1 (1970).
11. N. Kh. Akhmadeev and R. I. Nigmatulin, "Shocks and phase transformations in iron," Zh. Prikl. Mekh. Tekh. Fiz., No. 5 (1976).
12. N. Kh. Akhmadeev, "Analysis of one-dimensional flows during detonations of condensed substances," Tr. Nauchn. Issled. Inst. Mater. Vilnius. Gos. Univ., No. 21 (1975).
13. R. I. Nigmatulin and N. Kh. Akhmadeev, "Propagation of nonstationary shock and detonation waves in condensed media with physicochemical transformations," Report of the Scientific-Research Institute of Mechanics, Moscow State Univ. [in Russian], No. 1819 (1976).
14. A. G. Ivanov, S. A. Novikov, and Yu. I. Tarasov, "Spall phenomena in iron and steel, caused by rarefaction shock interaction," Fiz. Tverd. Tela, 4, No. 1 (1962).
15. A. P. Rybakov, "Spalls in steel under loading by using a sheet high-explosive charge and impact by a plate," Zh. Prikl. Mekh. Tekh. Fiz., No. 1 (1977).
16. R. I. Nigmatulin, N. Kh. Akhmadeev, and I. N. Kholin, "Physicochemical processes in solids under explosive loading," in: Nonlinear Deformation Waves [in Russian], Tallin (1978).